An interdimensional correlation framework for realtime estimation of six degree of freedom target motion using a single x-ray imager during radiotherapy

D T Nguyen[1] , J Bertholet[3] , J-H Kim[1] , R O'Brien[1] , J T Booth[2] , P R Poulsen[3] and P J Keall[1]

1 Radiation Physics Laboratory, Sydney Medical School, The University of Sydney, Sydney, Australia

2 Northern Sydney Cancer Centre, Royal North Shore Hospital, Sydney, Australia

3 Department of Oncology, Aarhus University Hospital, Aarhus, Denmark

Corresponding Author : Doan Trang Nguyen, E-mail: d.nguyen@sydney.edu.au

Keywords: intrafraction tumour motion, real-time motion monitoring, intrafraction six degrees-of-freedom motions, tumour rotations, radiotherapy

Acknowledgments

This work is funded by a Cancer Australia grant (Priority-driven Collaborative Cancer Research Scheme) (APP1085360). Author P Keall is funded by an Australian NHMRC Senior Principal Research Fellowship. We especially thank the Department of Radiation Oncology at Aarhus University Hospital (Denmark) for their generosity in sharing anonymised tumour trajectories which was used in this paper for evaluating our novel algorithm.

Abstract

Increasing evidence suggests that intrafraction tumour motion monitoring needs to include both 3D translations and 3D rotations. Presently, methods to estimate the rotation motion require the 3D translation of the target to be known first. However, ideally, translation and rotation should be estimated concurrently. We present the first method to directly estimate six-degree-of-freedom (6DoF) motion from the target's projection on a single rotating x-ray imager in real-time.

This novel method is based on the linear correlations between the superior–inferior translations and the motion in the other five degrees-of-freedom. The accuracy of the method was evaluated in silico with 81 liver tumour motion traces from 19 patients with three implanted markers. The ground-truth motion was estimated using the current gold standard method where each marker's 3D position was first estimated using a Gaussian probability method, and the 6DoF motion was then estimated from the 3D positions using an iterative method.

The 3D position of each marker was projected onto a gantry-mounted imager with an imaging rate of 11 Hz. After an initial 110° gantry rotation (200 images), a correlation model between the superior–inferior translations and the five other DoFs was built using a least square method. The correlation model was then updated after each subsequent frame to estimate 6DoF motion in real-time.

The proposed algorithm had an accuracy (±precision) of -0.03 ± 0.32 mm, -0.01 ± 0.13 mm and 0.03 ± 0.52 mm for translations in the left–right (LR), superior–inferior (SI) and anterior–posterior (AP) directions respectively; and, $0.07 \pm 1.18°$, $0.07 \pm 1.00°$ and $0.06 \pm 1.32°$ for rotations around the LR, SI and AP axes respectively on the dataset.

The first method to directly estimate real-time 6DoF target motion from segmented marker positions on a 2D imager was devised. The algorithm was evaluated using 81 motion traces from 19 liver patients and was found to have sub-mm and sub-degree accuracy.

1. Introduction

In current radiation therapy, image guided radiation therapy (IGRT) is routinely applied at the start of treatment to align the target with its planned position. However, tumours in the thorax, abdomen and pelvis are not static during treatment. Hence, methods to monitor tumour motion during treatment are highly desirable, even more so with dose escalation and hypofractionation.

A number of different intrafraction real-time guidance methods have been used during prostate cancer treatments. Systems such as CyberKnife (Accuray, Sunnyvale, CA) and the real-time tracking radiotherapy (RTRT) system use real-time kilovoltage (kV) images from two (CyberKnife) or four (RTRT system) orthogonal room-mounted imagers to track the prostate position based on segmented positions of implanted fiducial markers (Shimizu et al 2000, Shirato et al 2000, 2003, Kitamura et al 2002, King et al 2009, Sazawa et al 2009). Calypso (Varian, Palo Alto, CA) (Kupelian et al 2007) and RayPilot (Micropos, Gothenburg, Sweden) (Castellanos et al 2012) utilise implanted electromagnetic transponders, transmitting positional signals to an external receiver. Emerging real-time guidance technologies include ultrasonography (Ballhausen et al 2015) and integrated magnetic resonance imaging (MRI)-radiation therapy systems (Fallone et al 2009, Raaymakers et al 2009). Common to all these methods is the need for additional dedicated and typically expensive equipment to perform the real-time guidance.

Ideally, real-time image guidance would be performed using a standard linear accelerator (linac) without relying on additional hardware. To this end, a number of algorithms have been proposed for the purpose of estimating the target's position in 3D based on its location on a 2D image, which can be acquired using a linear accelerator gantry mounted kilovoltage (kV) x-ray imager system. An apparent advantage of utilising the kV imager is that: most modern linear accelerators have a kV imager, mounted orthogonally to the treatment beam. However, as the target position on the kV imager only contains 2D information, a 2D $\rightarrow$ 3D target position conversion is often required. The sparse information renders the problem of solving for the target's 3D position ill-posed, hence, some a priori knowledge or assumption is usually required.

1.1. The problem of 2D $\rightarrow$ 3D estimation

Poulsen et al (2008b) proposed a maximum likelihood estimation (MLE) algorithm to estimate the target's 3D position assuming a Gaussian distribution, which can be built after a learning arc. This solution has been clinically implemented as the kilovoltage intrafraction monitoring (KIM) system, and is currently being trialled for real-time tumour motion guidance in a pilot clinical trial and a multi-centre clinical trial (Keall et al 2016, Nguyen et al 2017). Recently, a Bayesian method to estimate the proper distribution of the target was also proposed (Li et al 2011), which does not assume Gaussian distribution and hence may be more accurate in estimating the target's respiratory motion as the thoracic tumour motions are complicated and can be asymmetrical as well as hysteric.

Other 2D → 3D methods that do not follow the probabilistic approach have also been proposed. For Cone Beam CT (CBCT) trajectories reconstruction, the positions of the target in 3D can be estimated using phase-binning, and linear interpolation, assuming the target's position in 3D does not change much within each respiratory bin (Becker et al 2010, Park et al 2012). However, this method requires all projections to be collected before 2D → 3D estimation and hence, is not suitable for real-time target positional estimation during treatment.

A different approach for 2D → 3D estimation is to make use of interdimensional correlation (IDC), which works for two reasons: (1) thoracic tumour motion in the anterior–posterior (AP) and left–right (LR) are correlated to its motion in the superior–inferior (SI) direction; and (2) as the gantry rotates around the patient, the SI position of the tumour is always visible on the kV images. Poulsen et al (2008a) implicitly incorporated IDC into their MLE of a Gaussian distribution. Other authors have shown that IDC can be used exclusively for 2D → 3D estimation, i.e without probability estimation, including the works of Cho et al (2012) and Chung et al (2016). An advantage of this method is that it can be extended to include the signal from an external surrogate, which is also correlated with the 3D motion of the target. Additionally, the linear model of IDC could be expanded to include state-augmentation to account for hysteresis in thoracic tumour motions (Ruan et al 2008).

1.2. The problem of 2D → 6D estimation

Increasing evidence suggests that intrafractional tumour motion corrections should be applied for both tumour translations and tumour rotations (Rijkhorst et al 2009, Wu et al 2011, Amro et al 2013). Retrospective post-treatment calculations of tumour rotations have shown that the rotations could be significant for both prostate and lung tumours (Aubry et al 2003, Amro et al 2013). Dosimetrically, uncorrected prostate rotations of 15° can result in a 12% under dose to the tumour (Rijkhorst et al 2009). Tumour rotation estimation using KIM has been developed using the iterative closest point (ICP) algorithm (Tehrani et al 2013). This method has been used retrospectively to quantify translational and rotational motion for prostate and lung cancers (Huang et al 2015) and liver cancer (Bertholet et al 2016). A disadvantage of this method is that the rotational motions are solved after the translational motions as the ICP algorithm requires target positions in 3D.

In this work, we propose a novel method that expands upon the 2D → 3D IDC formalism to solve for six degrees of freedom in one step. The rationale behind this novel method is supported by the works of Huang et al (2015) and Bertholet et al (2016) that revealed strong correlations between the rotational motions and the superior–inferior translational motion in both lung and liver tumours. The accuracy and precision of the proposed algorithm are evaluated in silico with patients' tumour liver traces during CBCT scans prior to radiotherapy as described in Bertholet et al (2016).

This paper describes a direct method for estimating real-time 6DoF target motion from the target's positions on a 2D imager that is mounted on the gantry of a standard linac. Previous efforts to calculate 6DoF motion from the target's 2D positions were done in two steps: (i) estimating the 3D position of each point of the target; and (ii) calculating the 6DoF motion by iteratively minimising the sum of squared differences in estimated and measured 3D positions of the points of the target (Tehrani et al 2013, Huang et al 2015, Bertholet et al 2016). The implication of the prior work is that if errors occurs in the first step, the rotation estimation can become erroneous as well. The presented algorithm can be used to estimate 6DoF tumour motion affected by the breathing motion from 2D kV images in real-time. The method is thus applicable for use on standard-equipped modern linacs.

2. Methods

In this section, we first describe the formalism of a novel method for estimating 6DoF motion from 2D projection of a target using the least square method. Then, we describe the VMAT simulation used to comprehensively evaluate the proposed algorithm, based on the patients' liver data, acquired in a clinical trial at the Aarhus University Hospital. Throughout this paper, we use the IEC 61217 coordinate system to describe the patient's motion relative to the treatment beam.

2.1. The 2D → 6D-IDC formalism

2.1.1. The forward problem: 6D → 2D.

Finding a unique solution for the 6DoF motion of a target provided its projection in 2D is an inverse problem. To facilitate the description of this inverse problem, it helps to first describe the forward problem: if we know the target's 6DoF motions with respect to a reference, what is the projection of the object on a rotating kV imager?

In the Euclidean coordinates system, the rotational and translational position of a target $\boldsymbol{M}$ (where $\boldsymbol{M}$ consists of n number of points $\boldsymbol{M} = \begin{pmatrix} x_1 & x_2 & x_n \\ y_1 & y_2 & y_n \\ z_1 & z_2 & z_n \end{pmatrix} = \begin{pmatrix} \boldsymbol{x} \\ \boldsymbol{y} \\ \boldsymbol{z} \end{pmatrix}$) at time ($t$) with respect to a referenced position $\boldsymbol{M}_{\mathbf{ref}}$ is defined as:

$$\begin{pmatrix} \boldsymbol{x} \\ \boldsymbol{y} \\ \boldsymbol{z} \end{pmatrix} = \boldsymbol{R} \cdot \begin{pmatrix} \boldsymbol{x}_{\mathrm{ref}} \\ \boldsymbol{y}_{\mathrm{ref}} \\ \boldsymbol{z}_{\mathrm{ref}} \end{pmatrix} + \begin{pmatrix} T_{r\_x} \\ T_{r\_y} \\ T_{r\_z} \end{pmatrix} \quad (1)$$

where $\boldsymbol{R}$ is the rotational matrix:

$$R = R_x R_y R_z =$$
$$\begin{bmatrix} \cos\beta\cos\gamma & -\cos\beta\sin\gamma & \sin\beta \\ \cos\alpha\sin\gamma + \sin\alpha\sin\beta\cos\gamma & \cos\alpha\cos\gamma - \sin\alpha\sin\beta\sin\gamma & -\sin\alpha\cos\beta \\ \sin\alpha\sin\gamma - \cos\alpha\sin\beta\cos\gamma & \sin\alpha\cos\gamma + \cos\alpha\sin\beta\sin\gamma & \cos\alpha\cos\beta \end{bmatrix} \quad (1.1)$$

where $\varphi = (\alpha, \beta, \gamma)$ are the angles describing the rotation of the object around the axes ***x***, ***y*** and ***z***, respectively. Note that the vector $T_r = \left(T_{r-x}, T_{r-y}, T_{r-z}\right)^T$ is merely a mathematical by-product of the rotation equation to accurately relate a 3D object with coordinates (***x***, ***y***, ***z***) with its referenced coordinates $(x_{ref}, y_{ref}, z_{ref})$. The vector ***Tr*** on its own does not provide the translational motion information. The real translational vector is defined as simply a vector difference between the current centroid of the object and its referenced centroid coordinates:

$$T = \bar{M}_t - \bar{M}_{ref} = \begin{pmatrix} T_x \\ T_y \\ T_z \end{pmatrix} = \begin{pmatrix} \bar{x} \\ \bar{y} \\ \bar{z} \end{pmatrix} - \begin{pmatrix} \bar{x}_{ref} \\ \bar{y}_{ref} \\ \bar{z}_{ref} \end{pmatrix} \quad (1.2)$$

Given the object ***M*** with the 3D coordinates (***x***, ***y***, ***z***), we can find its projected position (***x*****p**, ***y*****p**) on the kV imager when the linac gantry is at a certain angle ***θ*** with the following projection equation:

$$P(x, y, z|\theta) = \begin{pmatrix} x_p \\ y_p \end{pmatrix}(\theta) = \frac{\mathrm{SID}}{\mathrm{SAD} - (x \cdot \cos\theta + z \cdot \sin\theta)} \begin{pmatrix} x \cdot \sin\theta & -z \cdot \cos\theta \\ & y \end{pmatrix} \quad (2)$$

where SID is the source-to-imager distance and SAD is the source-to-axis distance, i.e. the distance between the kV x-ray source to the radiation isocentre

Thus, from equations (1) and (2), we can determine the position of aa target projected onto the kV imager if the rotational matrix ***R*** and the vector ***Tr*** are known. The reference position ***M*****ref** in the context of external beam radiotherapy can be determined as the tumour position in the planning CT.

2.1.2. The inverse problem: 2D → 6D.

Conversely, to solve for the matrix ***R*** and the vector ***Tr*** given only the projected positions $\begin{pmatrix} x_p \\ y_p \end{pmatrix}$ of the target is an ill-posed problem. However, given three or more points in the target ***M***, a solution can be found numerically, providing *a priori* knowledge. In this paper, our *prior* is that there is a linear correlation between the translational and rotational components of the object's motion (Huang *et al* 2015, Bertholet *et al* 2016). Additionally, we also assume that the target moves rigidly, without any deformations.

If the translational and rotational components of the target's motions are linearly correlated, the following equation can be assumed:

$$\left(\widehat{T}_r;\widehat{\varphi}\right)=\begin{pmatrix}\widehat{T}_{r_x}\\ \widehat{T}_{r_y}\\ \widehat{T}_{r_z}\\ \widehat{\alpha}\\ \widehat{\beta}\\ \widehat{\gamma}\end{pmatrix}(t)=\begin{pmatrix}a_x\\ a_y\\ a_z\\ a_\alpha\\ a_\beta\\ a_\gamma\end{pmatrix}\cdot y(t)+\begin{pmatrix}b_x\\ b_y\\ b_z\\ b_\alpha\\ b_\beta\\ b_\gamma\end{pmatrix}=\boldsymbol{a}y(t)+\boldsymbol{b} \tag{3}$$

where $y(t)$ is the target's coordinate in the y (superior–inferior) direction and the vectors $\boldsymbol{a}$ and $\boldsymbol{b}$contain all scalars. Equation (3) relates all the components of equation (1) with the target's y-coordinate. This is advantageous because the gantry and kV imager rotate around the y-axis. In fact, from the equation (2), we have:

$$y\left(t\,|\theta\right)=\frac{\mathrm{SAD}-\left(x(t)\cdot\cos\theta+z(t)\cdot\sin\theta\right)}{\mathrm{SID}}y_{\mathrm{p}}(t). \tag{4}$$

If we assume the quantity $\left(x(t)\cdot\cos\theta+z(t)\cdot\sin\theta\right)$ in equation (4) to be much smaller than SAD, which is realistic because SAD is normally 1000 mm in most clinical linac systems while the distance between the target position and the gantry rotation axis is typically small. This is because in reality, the radiation isocentre will either in or very close to the tumour, i.e. our target. In some cases, implanted markers are to be tracked instead of the tumour, which are usually implanted in the vicinity of the tumour. Then $y(t)$ can be approximated as:

$$y(t)=\frac{\mathrm{SAD}}{\mathrm{SID}}y_{\mathrm{p}}(t). \tag{4.1}$$

As equation (4.1) enables a relatively accurate estimation of $y(t)$, the scalar vectors $\boldsymbol{a}$ and $\boldsymbol{b}$ can hence be estimated using the least squares method, similar to methods described by Ruan *et a l*(2008), Cho *et al* (2012) and Chung *et al* (2016), with some modifications: firstly, from equation (3), $\left(\widehat{T}_r;\widehat{\varphi}\right)(t)$ can be estimated from $y(t)$. Consequently, we can compute the estimated coordinates $\begin{pmatrix}\widehat{x}\\ \widehat{y}\\ \widehat{z}\end{pmatrix}$ using equation (1), which can then be used to compute the estimated projected coordinates $\begin{pmatrix}\widehat{x}_{\mathrm{p}}\\ \widehat{y}_{\mathrm{p}}\end{pmatrix}$ by applying equation (2) to $\begin{pmatrix}\widehat{x}\\ \widehat{y}\\ \widehat{z}\end{pmatrix}$. The cost function of the Euclidean distance between $\begin{pmatrix}\widehat{x}_{\mathrm{p}}\\ \widehat{y}_{\mathrm{p}}\end{pmatrix}$ and the actual coordinates of the target $\begin{pmatrix}x_{\mathrm{p}}\\ y_{\mathrm{p}}\end{pmatrix}$ can then be computed as:

$$C=\sum_{f=0}^{f=F}\sum_{m=1}^{n}\sqrt{\left(x_{p\_m}^{f}-\widehat{x}_{p\_m}^{f}\right)^2+\left(y_{p\_m}^{f}-\widehat{y}_{p\_m}^{f}\right)^2}. \tag{5}$$

In the simulation, the number of points is $n=3$. The parameter F indicates the number of image frames used to calculate the cost function, which is explained in further details in the next

section. Finally, the vectors $\boldsymbol{a}$ and $\boldsymbol{b}$ can be estimated by minimizing the cost function $\boldsymbol{C}$, given $\begin{pmatrix} x_p \\ y_p \end{pmatrix}(t)$, in the least square sense:

$$(\boldsymbol{a}, \boldsymbol{b}) = \arg\min \|C\|_2. \quad (6)$$

Since equation (4.1) is only an approximation of equation (4), we iteratively refine the solution, as shown in the pseudo-codes in figure 1.

2.2. In silico simulation

The flowchart in figure 2 summarises in silico simulation and data processing to evaluate the accuracy of the proposed 6D-IDC algorithm.

2.2.1. Simulated real-time implementation.

2.2.1.1. Learning phase.

The 6D-IDC algorithm was then used to estimate 6DoF motion using only information from the projected positions of the markers on each image frame, as described in section 2.1. The first 6D-IDC model was built after 200 imaging frames ($F = 200$), equivalent to 110° of gantry rotation. For the first model, it was found that using 6 iterations allows the solution to converge for all the test trajectories with the difference in the sum of square error criterion set at 10^{-6} mm.

2.2.1.2. Simulate real-time estimation with 3 markers available.

After the learning phase, with the positions of all three markers available in each new frame, the correlation model was updated using all the historical 2D data up to the current frame. When updating the model, only one iteration of optimisation was used, instead of 6 as described in the algorithm in figure 1, and the least square optimisation was started at the last found solution for the correlation vectors $\boldsymbol{a}$ and $\boldsymbol{b}$. During the update phase, the least square solver used the solution from the last time point. This effectively gives it a 'warm start'. Thus, the six iterations were not necessary and one iteration was sufficient to have the solution converge.

2.2.1.3. Simulate real-time estimation with only 1 marker available.

Once the correlation model had been built after the learning phase, equation (3) enabled 6DoF motion estimation based on the projected position yp of one marker, assuming at least one of three markers projection was available in the new imaging frame. In this case, the correlation model was not rebuilt. Thus, the estimation is based solely on the pre-computed correlation model. The worst case scenario was simulated, in which only the position of 1 marker was available for 6DoF estimations after the correlation model was built. Note that during the learning phase, all three markers positions were used to build the model.

2.2.2. VMAT simulation.

In order to test the accuracy of the 6D-IDC algorithm estimated 6DoF motion, for each trace in the ground-truth dataset, the ground-truth 3D positions of the markers were projected onto the imager using equation (2). The SAD and SID value were set at 1000 mm and 1800 mm, respectively. For each simulation, the gantry started at 180° and rotated counter-clockwise at 6° s−1 to simulate a full rotation VMAT treatment.

2.2.3. Ground-truth data descriptions.

A dataset of 29 patients with three fiducials implanted near the tumour in the liver for image guided radiotherapy, first described by Bertholet et al (2016), was used in our in silico simulation. Each patient was treated with stereotactic body radiation therapy (SBRT), receiving treatment in 3–6 fractions. In each fraction, each patient's 1 to 3 cone beam CBCT scans (11 fps, 125 kV, 80 mA, 13 ms) were acquired. The fiducials were segmented in each image. We furthermore rejected traces where the data were not continuous for at least 50 s. This is because the simulation aims to mimic real-time treatment to assess the algorithm's accuracy for realistic intrafraction conditions. If there were more than one segments of continuous data within one fraction, each continuous segment was used independently. Overall, the refined dataset contained 81 traces from 19 patients. The overall flow chart of the simulation is shown in figure 2. The range of 6DoF motions in this dataset are shown in figure 3.

The ground truth 6 DoF motion data were computed in two steps. The 2D $\rightarrow$ 3D estimation of each marker's position in each image frame was computed using the method of Poulsen et al (2008b), which has been measured to have sub-mm accuracy (Poulsen et al 2008b, Keall et al 2016). From the imaging frames with all three markers successfully segmented, the 6DoF motions of the target were calculated using the ICP algorithm (Tehrani et al 2013), which computed the 6DoF motions from individual 3D coordinates of the three markers. The accuracy of this method in estimating the rotation motions during radiotherapy were evaluated and quantified by Kim et al (2016) and found to be accurate within 1°. The positions of the markers at the first frame of imaging in each fraction were used as the reference positions for 6DoF calculation as it was the intrafraction 6DoF motions that were of interest.

2.2.4. Analysis of simulation results.

The error of the 6D-IDC algorithm was defined as the difference between 6DoF motions estimated with 6D-IDC and the 6DoF ground-truth motion.

We analysed the factors affecting the accuracy of 6D-IDC, including:

1. Deformation: estimated by the change in the area of the triangle, that was formed by the 3 markers, in 3D in each frame, compared with the referenced area.

2. Absolute magnitude of motion in each DoF: the absolute value of 6DoF motions in each frame relative to planned marker position.

3. Linear correlation between motion in each DoF and the motion of the SI direction: defined by the absolute value of the Pearson's linear correlation value (ρ) computed between the motion in each DoF and the motion in SI for each tested trace.

The effect of each of the aforementioned factors on the accuracy was quantified by calculating the Pearson's correlation value (ρ) between the absolute value of the error in each DoF and the tested parameter, except for the third factor, linear correlation value. The correlation between the maximum value of error in estimating 6DoF motion and the linear correlation value of each DoF was used instead because linear correlation value was a trace-specific value.

The 6D-IDC algorithm, in silico simulation and analyses of the results were implemented in Matlab (Mathworks, MA, USA).

3. Results

For this section, the translational motion is denoted by its axis of motion, e.g. translation motion in LR is denoted as 'LR'. The rotational motion is denoted by an 'r' before its axis of rotation, e.g. rotation motion around the SI axis is denoted as 'rSI'. This is simply for clarity in figures.

3.1. Accuracy of 6D-IDC estimation with three markers available

Figure 4 shows a comparison of 6DoF motion estimated using 6D-IDC and the ground truth motion used in the simulation. The means and standard deviations of the differences are summarised in table 1. The mean of error in the 6DoF are under 0.1 mm and 0.1° across 81 motion traces from 19 patients. The standard deviations of error for 6D-IDC estimated motion are less than 1 mm for translational motion and less than 1.5° for rotational motion. This result is a pooled analysis across 53736 imaging frames of the 81 liver motion traces from 19 patients. The boxplot of the overall error is shown in figure 5.

Figure 6 shows the boxplot of the mean error of 6D-IDC estimations compared with ground-truth 6DoF motion for each of the 81 tested traces. From figure 6, it can be observed than even though there are outliers of error up to 20°, as seen in figure 5, in 95% of cases, the mean error of 6D-IDC estimated motion of each trace are within 1 mm and 1°. A typical example of one case where such large outliers are present, is shown in figure 7. As depicted in figure 7, some of the outliers were caused by sudden motions, such as coughing, which altered the linear relationship between the motion in SI and motions in the other DoFs.

3.2. 6DoF motion estimation with only one marker projection available after a learning arc

Table 2 shows the summary statistics of the error of 6DoF motion estimation by the 6D-IDC method if only one marker projection is available after the learning arc of 110°. In all 6DoF estimation, the mean and standard deviation of errors are higher when only one marker projection is used for estimation, compared with when all three markers projections are used, as shown in figure 8. Figure 9 shows a case in which 6D-IDC is as accurate with one marker (figure 9(I-A)) as with three markers (figure 9(I-B)) and

another case in which 6D-IDC with one marker is less accurate (figure 9(II-A)) than with three markers (figure 9(II-B)).

3.3. Factors affecting 6D-IDC accuracy

Figures 10 and 11 are the scatter plots of the error between 6D-IDC estimated motions in each DoF as a function of the magnitude of deformation, assessed by the variation in the area of the triangle subtended by the markers (figure 10) and the absolute value of motion (figure 11).

The magnitude of the deformation seen in the ground-truth dataset had little effect on the accuracy of the 6D-IDC algorithm (figure 10). From the scatter plots in figure 10, the relationship between the magnitude of error and the change in area in each frame was weak in all six DoFs. The computed Pearson correlation coefficients shows that the error in the translational SI direction has the highest correlation with the change in area ($\rho = 0.41$), followed by the error in the translational AP direction ($\rho = 0.28$) and the error in the rotation around the LR axis ($\rho = 0.22$).

The absolute magnitude of ground-truth motion, which includes systematic offsets, does not have any effect on the magnitude of 6D-IDC error in estimating translational motion; all the Pearson's correlation ρ values for the translation motion are less than 0.1 (figure 11). The magnitude of the rotational motions are weakly correlated with the magnitude of the error (figure 11) with rSI and rAP having ρ values less than 0.3 and rLR having a ρ value of 0.42.

Figure 12 shows scatter plots of the maximum of error and the linear correlation between each DoF motion and the translational SI motion for all tested traces. A strong correlation is found in the AP translation motion and the rotation around the LR axis (rLR), with Pearson's correlation ρ values of -0.6 for AP and -0.5 for rLR. A negative Pearson's correlation indicates a negatively correlated relationship. However, in all other DoF motions, no correlation or very weak correlation can be observed. From figure 12, it can also be observed that most of the outliers occurred with weak correlation with SI (<0.2), especially in translation motions in AP and rLR and rAP rotation motion.

4. Discussion

This paper describes a method to directly estimate 6DoF target motion from segmented marker positions on a 2D imager that is mounted on the gantry of a standard linac. This algorithm can be implemented for real-time estimation of 6 DoF motions of a tumour on a linac together with a marker segmentation algorithm. Previous efforts to calculate 6DoF motion from the target's 2D positions were performed in two steps: (i) estimating the 3D position of the target; and (ii) calculating the 6DoF motion by iteratively minimising the sum of squared differences in estimated and measured 3D positions of the target (Tehrani et al 2013, Huang et al 2015, Bertholet et al 2016). The presented method utilises the interdimensional correlation in the translation in SI direction with other 5 degrees of freedom motions as an a priori, which was found to exist for liver and lung traces in previous studies (Huang et al 2015, Bertholet et al 2016). This new method, named 6D-IDC, has been evaluated in a series of in silico simulations with liver SBRT patients' 6DoF trajectories.

Compared with the ground-truth 6DoF motion, assumed as the current standard for estimating 6DoF motions, the 6D-IDC algorithm performed equivalently well, with sub-mm and sub-degree accuracy on the tested dataset. The accuracy (mean) and precision (standard deviation) of the 6D-IDC method in estimating translation motions of the tested dataset were sub-mm, which is comparable to previously reported 2D–3D accuracy of probability-based methods in similar simulations with thoracic/abdominal tumour trajectories (Poulsen et al 2008b, Li et al 2011).

The algorithm performed better, with both higher accuracy and precision, when the projections of all three markers were available (figure 8). However, with only one marker projection information available after the learning arc, the algorithm still gives sub-mm and sub-degree mean error in all 6 DoFs. This is particularly advantageous for real-time applications as all three markers may not be visible or reliably detected on a projection at all times. Furthermore, the algorithm can also be used with MV tracking provided the initial correlation model is built during initial CBCT imaging. The standard deviations of error for the 3D translations are under 1 mm while the standard deviations of error for the 3D rotations are under 2° using only one marker projection. This is compared to a maximum standard deviation of error of 0.52 mm for translation and 1.3° for rotation error estimation when three markers are available. This is not surprising as the correlation model does not get updated when only one marker projection is available while it is constantly updated when all three markers are available. In the cases when occasionally all three markers are available while only one of the markers projection are available most of the time, the algorithm can be optimised by updating the correlation model in the occasions when all three markers projections are available to improve its performance.

The presented 6D-IDC algorithm employs solving the correlation matrix in a least square sense. This formalism of solving 6DoF motion from the target's projection on an imager is a scalable solution. In our simulation, three points, i.e. markers, were used. Three is the lowest number of points to describe the target that allows the algorithm to uniquely determine the rotation and translation of the object. The algorithm is capable of solving for the 6DoF motion of a target comprised of a larger number of points, such as situations with four or more markers, or the segmented tumour on a projection image.

The perspective-n-point problem in computer vision can be used to solve for the 6DoF information of an object, provided three or more points are available on an image taken by a calibrated camera (kV imaging system in this case) and the distances between these points are known. Haralick et al (1994) describes a range of algorithms to solve for the 3D position of each point of the object in the case where only three points are available, from which the absolute orientation of the object can be determined. Thus, the perspective-n-point problem is in fact similar to the problem of determining 6DoF tumour motions of radiotherapy. Similar to the existing method (Tehrani et al 2013) to determine tumour translation and rotation from fluoroscopic 2D images, the perspective-n-point solves the translation and rotation in two steps. The 3D coordinates of each point must be solved before the absolute transformation matrix can be

determined (Haralick et al 1994). The advantage of our solution to solve for tumour motion during treatment is in the use of equation (3), which linearly models the correlation between motion in the SI direction and the other 5 degrees of freedom motions. Utilising equation (3), our algorithm is able to compute the rotation and translation of the target directly, without the need to solve for the 3D coordinates of each point separately. Furthermore, with equation (3), the 6D-IDC algorithm can be used to estimate 6DoF motion when only one marker is available provided the parameters of the correlation matrix are already computed during a learning arc where three or more markers are available. This feature sets this work apart from the prior works in the field.

The reported results were from an online scenario where the 6D-IDC algorithm estimated 6DoF motion on each new in-coming image, after a learning arc. The accuracy of the algorithm is likely to be better in a retrospective scenario. However, we were more interested in its performance in real-time as the main application for such an algorithm is intrafraction monitoring and as a positioning system for a tracking system. A learning arc of 110° was used in our simulation, which is less than the learning arc (120°) used in clinical application of the probability-based method by Poulsen et al (2008a) and Keall et al (2016). Additionally, Chung et al (2016) described a 3D IDC-based method and showed that a learning arc of at least 90° reduced the errors in estimating motions at the start of the trajectory. Similarly, we found that around 110° of learning arc provided a stable start for the 6D-IDC algorithm.

As shown in figures 4 and 7, the rotation motions calculated with 6D-IDC tend to be smoother and free of spikes, compared with rotation motions calculated with the ICP algorithm. This is because the ICP algorithm is sensitive to noise in the 3D positions of the object. That is, if one of the three markers moves due to the noise in the system, the ICP algorithm interpreted such movements as true motions and attempted to over-fit into its model. Meanwhile, the presented 6D-IDC algorithm attempted to find the best rotation and translation correlation parameters to minimise the error between the estimated position of the object and its projection on the imager. Effectively, performing the least square estimation on at least 200 points of data filtered the signal so as to mitigate noise in the estimated signal as well.

We investigated a number of factors that could influence the accuracy of the presented 6D-IDC algorithm, including deformation, quantified by the change in area of the triangle formed by the 3 markers in 3D, the magnitude of motion in 6DoF and the correlation between each DoF and the motion in SI. Among these three factors, it was found that the algorithm was robust against both deformation and both large rotation and translation motions, with low or very low Pearson's correlation values between the magnitude of error and any of the aforementioned values. However, the 6D-IDC algorithm was sensitive to the correlation value between each DoF and the motion in SI, especially in the AP and rLR direction. The outliers in the estimation errors of each DoF also occur more frequently at low correlation, as shown in figure 10. If the algorithm is to be implemented clinically, the correlation value can be used to assess the degree of its reliability in estimating 6DoF motion in each patient. In patients whose motions have low value of correlations, e.g. correlation with magnitude of less than 0.2, probability methods such as those described by Poulsen et al (2008b) and Li et al (2011) could be more accurate than the 6D-IDC method.

4.1. Limitations and future work

One limitation of this work is the inherent uncertainty of the ground-truth dataset. From the previous works (Poulsen et al 2008a, 2008b, Bertholet et al 2016, Keall et al 2016, Kim et al 2017), it has been shown that the uncertainty of the ground-truth data set is within 1 mm and 1°. Specifically, Kim et al (2017) showed experimentally on a phantom that estimation of 6DoF motions for prostate and lung tumour traces using the combination of the probability method and the ICP method has an accuracy of 1 mm and 1° as compared with kV/MV triangulation. Furthermore, the ground-truth data rejected 3D points that had an uncertainty of more than 1 mm, as described in Bertholet et al (2016). Although the uncertainty of the ground-truth dataset is low, it does affect the presented results. In the worst-case scenario, the reported error is an additive combination of the actual error inherent to our method and the inherent error within the ground-truth dataset. Data from a more independent source such as the electromagnetic system Calypso (Varian Medical System, Palo Alto, CA, USA) may provide a more reliable benchmarking dataset than the dataset used in this paper, e.g. in clinical trials such as (Booth et al 2016, Poulsen et al 2016). However, these clinical trials have not been completed and the data is not yet available.

In this paper, the 6D-IDC method was evaluated using in silico simulations for VMAT treatments. Due to the short duration of the continuous trajectories available in our dataset where all of the tested trajectories were less than 65 s in length, IMRT simulations were not carried out. As more data of intrafraction tumour motions of the thoracic and abdominal tumours with at least three points become available from the ongoing clinical trials, the algorithm will also be evaluated for IMRT treatments. The immediate next step is to further evaluate the accuracy of the algorithm in phantom experiments, paving the way to develop it as a clinical tool for real-time tumour motion management during treatment. Such a development would require the algorithm to be implemented together with a marker or markerless tumour segmentation algorithm.

5. Conclusion

This paper describes, to the best of our knowledge, the first method that is capable of directly estimating 6DoF target motion from the target's positions on a 2D imager that is mounted on the gantry of a standard linear accelerator. The accuracy of the algorithm was numerically evaluated using 81 liver tumour motion traces from 19 patients and found to be within sub-mm and sub-degree, with precision sub-mm and sub-1.5°. Requiring only images from a single rotating kV imaging system that is widely available in all modern linear accelerators, the described method can thus be used to estimate the real-time tumour 6DoF motion for real-time treatment adaptations.

References

Amro H, Hamstra DA, Mcshan D L, Sandler H, VinebergK, Hadley S and Litzenberg D 2013 The dosimetric impact of prostate rotations during electromagnetically guided external-beam radiation therapy Int. J. Radiat. Oncol. Biol. Phys. 85 230–6

Aubry J-F, Beaulieu L, Girouard L-M, Aubin S, Tremblay D, Laverdière J and Vigneault E 2003 Measurements of intrafraction motion and interfraction and intrafraction rotation of prostate by three-dimensional analysis of daily portal imaging with radiopaque markers Int. J. Radiat. Oncol. Biol. Phys. 60 30–9

Ballhausen H, Li M, Hegemann N-S, Ganswindt U and BelkaC 2015 Intra-fraction motion of the prostate is a random walk Phys. Med. Biol. 60 549–63

Becker N, SmithWL, Quirk S and Kay I 2010 Using cone-beam CT projection images to estimate the average and complete trajectory of a fiducial marker moving with respiration Phys. Med. Biol. 55 7439–52

BertholetJ, Worm E S, FledeliusW, Høyer M and Poulsen PR 2016 Time-resolved intrafraction target translations and rotations during stereotactic liver radiation therapy: implications for marker-based localization accuracy Int. J. Radiat. Oncol. Biol. Phys. 95 802–9

Booth J T, CailletV, Hardcastle N, O'brienR, SzymuraK, CrastaC, Harris B, HaddadC, Eade T and Keall P J 2016 The first patient treatment of electromagnetic-guided real time adaptive radiotherapy using MLC tracking for lung SABR Radiother. Oncol. 121 19–25

Castellanos E, Ericsson M H, Sorcini B, Green U, Nilsson S and Lennernäs B 2012 RayPilot—electromagnetic real-time positioning in radiotherapy of prostate cancer—initial clinical results Radiother. Oncol. 103 S433

Cho B, Poulsen PR, Ruan D, SawantA and Keall P J 2012 Experimental investigation of a general real-time 3D target localization method using sequential kV imaging combined with respiratory monitoring Phys. Med. Biol. 57 7395–407

Chung H, Poulsen PR, Keall P J, Cho S and Cho B 2016 Reconstruction of implanted marker trajectories from cone-beam CT projection images using interdimensional correlation modeling Med. Phys. 43 4643–54

Fallone B G, Murray B, Rathee S, Stanescu T, SteciwS, Vidakovic S, Blosser E and Tymofichuk D 2009 First MR images obtained during megavoltage photon irradiation from a prototype integrated linac-MR system Med. Phys. 36 2084–8

HaralickR M, LeeC-N, OttenbergK and Nölle M 1994 Review and analysis of solutions of the three point perspective pose estimation problem Int. J. Comput. Vis. 13 331–56

Huang C-Y, Tehrani J N, Ng JA, Booth J T and Keall P J 2015 Six degrees-of-freedom prostate and lung tumor motion measurements using kilovoltage intrafraction monitoring Int. J. Radiat. Oncol. Biol. Phys. 91 368–75

Keall P J et al 2016 Real-time 3D image guidance using a standard LINAC: measured motion, accuracy, and precision of the first prospective clinical trial of kilovoltage intrafraction monitoring guided gating for prostate cancer radiation therapy Int. J. Radiat. Oncol. Biol. Phys. 94 1015–21

Kim J, Nguyen D, Huang C, Fuangrod T, Caillet V, O'Brien R, Poulsen P, Booth J and Keall P 2017 Quantifying the accuracy and precision of a novel real-time 6 degree-of-freedom kilovoltage intrafraction monitoring (KIM) target tracking system Phys. Med. Biol. 62 5744–59

Kim J-H, Nguyen D T, HuangC-Y, O'BrienR, CailletV, Poulsen PR, Booth J T and Keall P 2016 Quantifying the accuracy and precision of six degree-of-freedom motion estimation for use in real-time tumor motion monitoring during radiotherapy The 58th Annual Meeting of the American Association of Physicists in Medicine, 2016. Medical Physics pp 3858–9

King CR, BrooksJ D, Gill H, Pawlicki T, CotrutzC and Presti JC 2009 Stereotactic body radiotherapy for localized prostate cancer: interim results of a prospective phase II clinical trial Int. J. Radiat. Oncol. Biol. Phys. 73 1043–8

Kitamura K et al 2002 Registration accuracy and possible migration of internal fiducial gold marker implanted in prostate and liver treated with real-time tumor-tracking radiation therapy (RTRT) Int. J. Radiat. Oncol. Biol. Phys. 62 275–81

Kupelian P et al 2007 Multi-institutional clinical experience with the Calypso System in localization and continuous, real-time monitoring of the prostate gland during external radiotherapy Int. J. Radiat. Oncol. Biol. Phys. 67 1088–98

Li R, Fahimian B P and Xing L 2011 A Bayesian approach to real-time 3D tumor localization via monoscopic x-ray imaging during treatment delivery Med. Phys. 38 4205–14

Nguyen D T, Kim J-H, O'Brien RT, Huang C-Y, Booth J T, Greer P, Legge K, Poulsen PR, Martin J and Keall P J 2017 The first clinical implementation of a real-time six degree of freedom tracking system during radiation therapy Radiother. Oncol. 123 37–42

Park JC et al 2012 Liver motion during cone beam computed tomography guided stereotactic body radiation therapy Med. Phys. 39 6431–42

Poulsen PR, Cho B and Keall P J 2008a A method to estimate mean position, motion magnitude, motion correlation, and trajectory of a tumor from cone-beam ct projections for image-guided radiotherapy Int. J. Radiat. Oncol. Biol. Phys. 72 1687–596

Poulsen PR, Cho B, Langen K, Kupelian P and Keall P J 2008b Three-dimensional prostate position estimation with a single x-ray imager utilizing the spatial probability density Phys. Med. Biol. 53 4331–53

Poulsen PR, Worm E S, Hansen R, Larsen L P, Grau C and Høyer M 2016 Respiratory gating based on internal electromagnetic motion monitoring during stereotactic liver radiation therapy: first results Acta Oncol. 54 1445–52

Raaymakers BW, Lagendijk JJW, Overweg J, Kok J G M, Raaijmakers AJ E, Kerkhof E M, Put RWV D, Meijsing I, Crijns S P M and Benedosso F 2009 Integrating a 1.5 T MRI scanner with a 6 MV accelerator: proof of concept Phys. Med. Biol. 54 N229

Rijkhorst E-J, LakemanA, Nijkamp J, BoisJ D, Herk MV, Lebesque JV and Sonke J-J 2009 Strategies for online organ motion correction for intensity-modulated radiotherapy of prostate cancer: prostate, rectum, and bladder dose effects Int. J. Radiat. Oncol. Biol. Phys. 75 1254–60

Ruan D, FesslerJA, BalterJ M, BerbecoRI, Nishioka S and Shirato H 2008 Inference of hysteretic respiratory tumor motion from external surrogates: a state augmentation approach Phys. Med. Biol. 53 2923–36

Sazawa A, Shinohara N, Harabayashi T, Abe T, Shirato H and Nonomura K 2009 Alternative approach in the treatment of adrenal metastasis with a real-time tracking radiotherapy in patients with hormone refractory prostate cancer Int. J. Urol. 16 410–2

Shimizu S, Shirato H, Kitamura K, Shinohara N, Harabayashi T, Tsukamoto T, Koyanagi T and Miyasaka K 2000 Use of an implanted marker and real-time tracking of the marker for the positioning of prostate and bladder cancers Int. J. Radiat. Oncol. Biol. Phys. 48 1591–7

Shirato H et al 2000 Physical aspects of a real-time tumor-tracking system for gated radiotherapy Int. J. Radiat. Oncol. Biol. Phys. 48 1187–95

Shirato H et al 2003 Feasibility of insertion/implantation of 2.0 mm-diameter gold internal fiducial markers for precise setup and real-time tumor tracking in radiotherapy Int. J. Radiat. Oncol. Biol. Phys. 56 240–7

Tehrani J N, O'Brien RT, Poulsen PR and Keall P 2013 Real-time estimation of prostate tumor rotation and translation with a kV imaging system based on an iterative closest point algorithm Phys. Med. Biol. 58 8517–33

Wu J, Ruan D, Cho B, Sawant A, Petersen J, Newell L J, Cattell H and Keall P J 2011 Electromagnetic detection and real-time DMLC adaptation to target rotation during radiotherapy Int. J. Radiat. Oncol. Biol. Phys. 82 e545–53

Table 1. Summary of error of 6DoF motion estimated with 6D-IDC using projected positions of three markers after 110° learning arc.

	Mean error	Standard deviation of error	(5th to 95th) percentile interval
LR (mm)	−0.03	0.32	(−0.55–0.50)
SI (mm)	−0.01	0.13	(−0.18–0.17)
AP (mm)	0.03	0.52	(−0.64–0.73)
rLR (°)	0.07	1.18	(−1.51–1.70)
rSI (°)	0.07	1.00	(−1.50–1.70)
rAP (°)	0.06	1.32	(−1.53–1.68)

```
for i = 1:k
    if (i==1)
       - Compute y using equation (4-1).
       - A and B initialised to unity vectors.
    else
       - Compute (T̂_r_x, T̂_r_y, T̂_r_z, α̂, β̂, γ̂) based on previous value of
       a,b.
       - Compute new rotation matrix with α̂, β̂, γ̂.
       - Compute new estimated centroid location.
       - Compute new y of estimated centroid location using
     equation (4).
    end
     -  Optimise the cost function C with new value of y to
       solve for A and B.
end
```

Figure 1. Pseudo-codes for refining vectors ***a*** and ***b*** estimations with 6D-IDC; $k = 6$ during learning phase and $k = 1$ during real-time update.

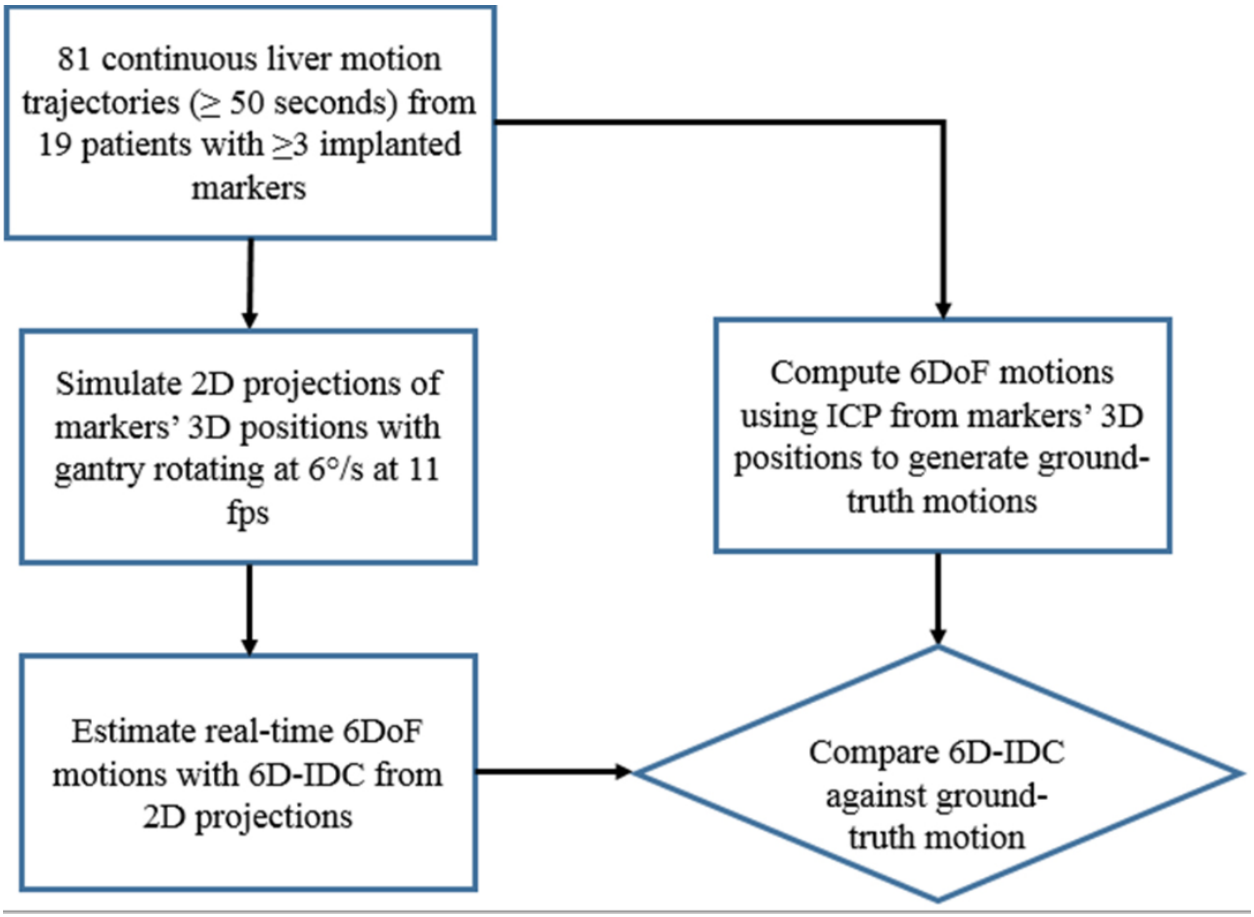

Figure 2. Flow chart of the *in silico* simulation for evaluating the accuracy of 6D-IDC.

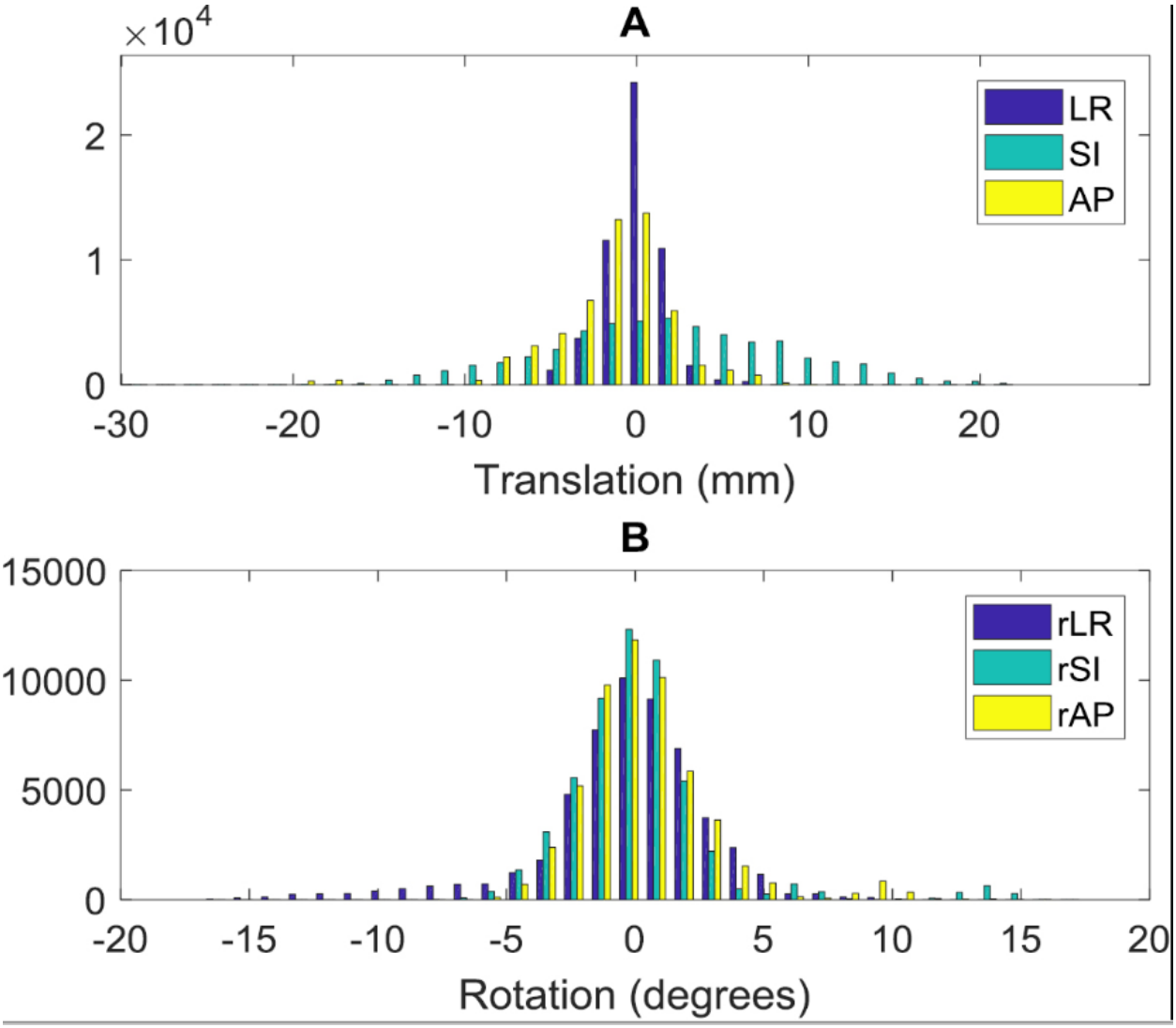

Figure 3. Histogram of six degrees of freedom motion in the ground-truth data, across 81 traces from 19 patients and 53736 frames. (A) Translational motion (LR: left–right, SI: superior–inferior, AP: anterior–posterior). (B) Rotational motion.

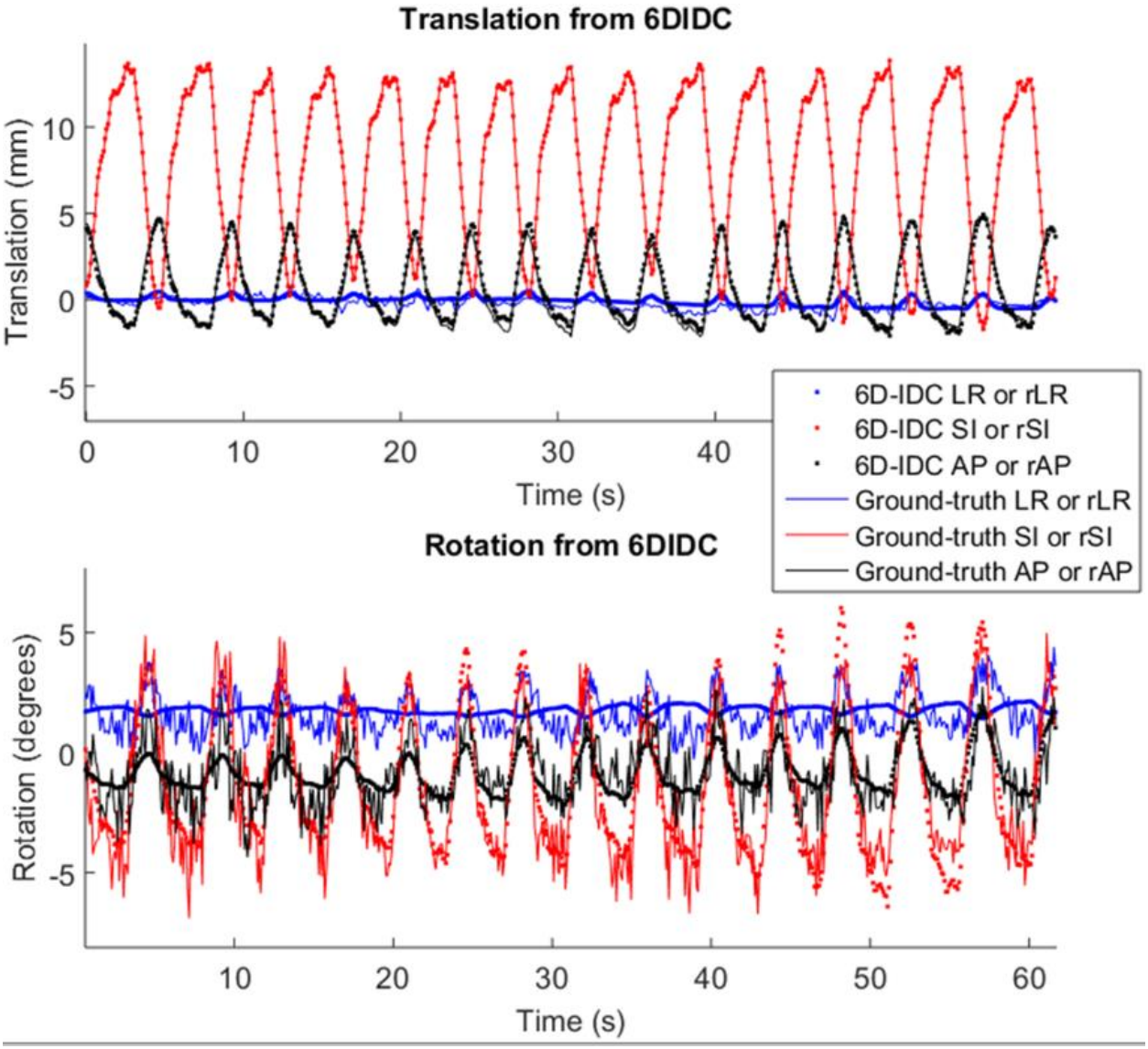

Figure 4. Six degree of freedom target motion successfully estimated with 6D-IDC compared to the ground truth. The data is from patient 26, fraction 3.

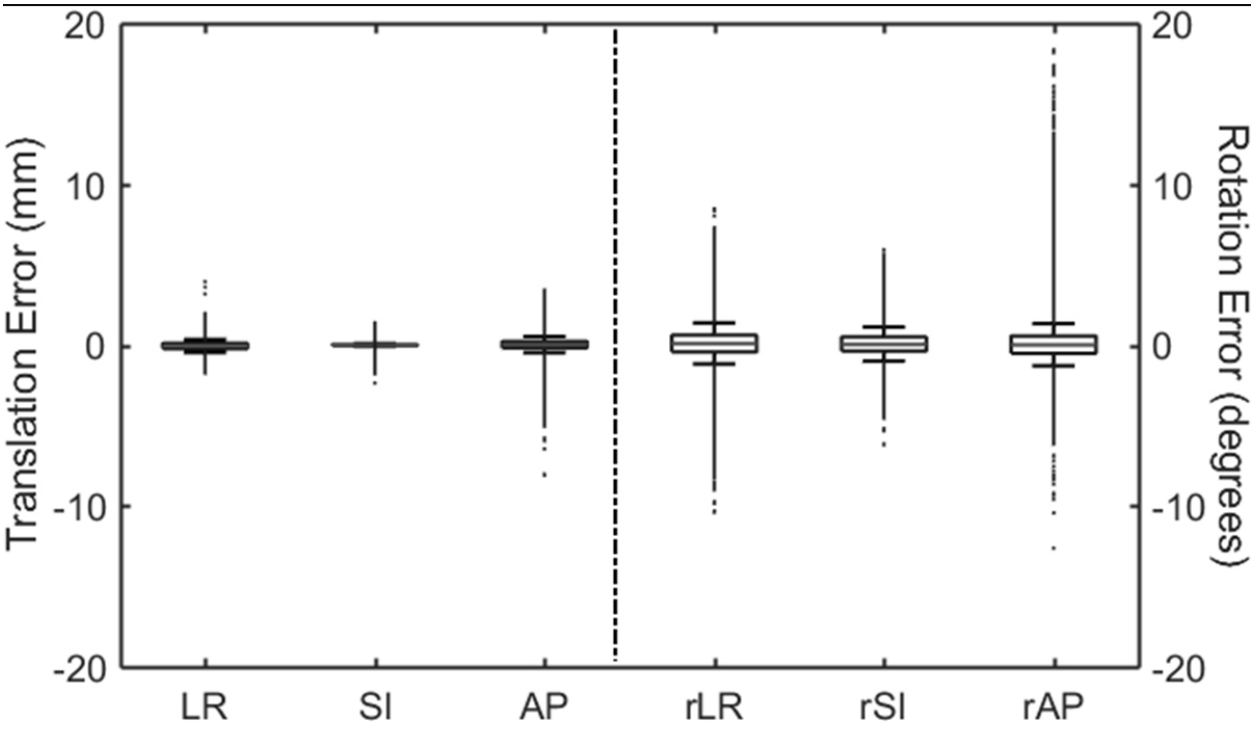

Figure 5. Boxplot showing the distributions of error in 6DoF between 6D-IDC estimations with three markers projections and ground-truth across 81 liver tumour traces from 19 patient with 53736 image frames.

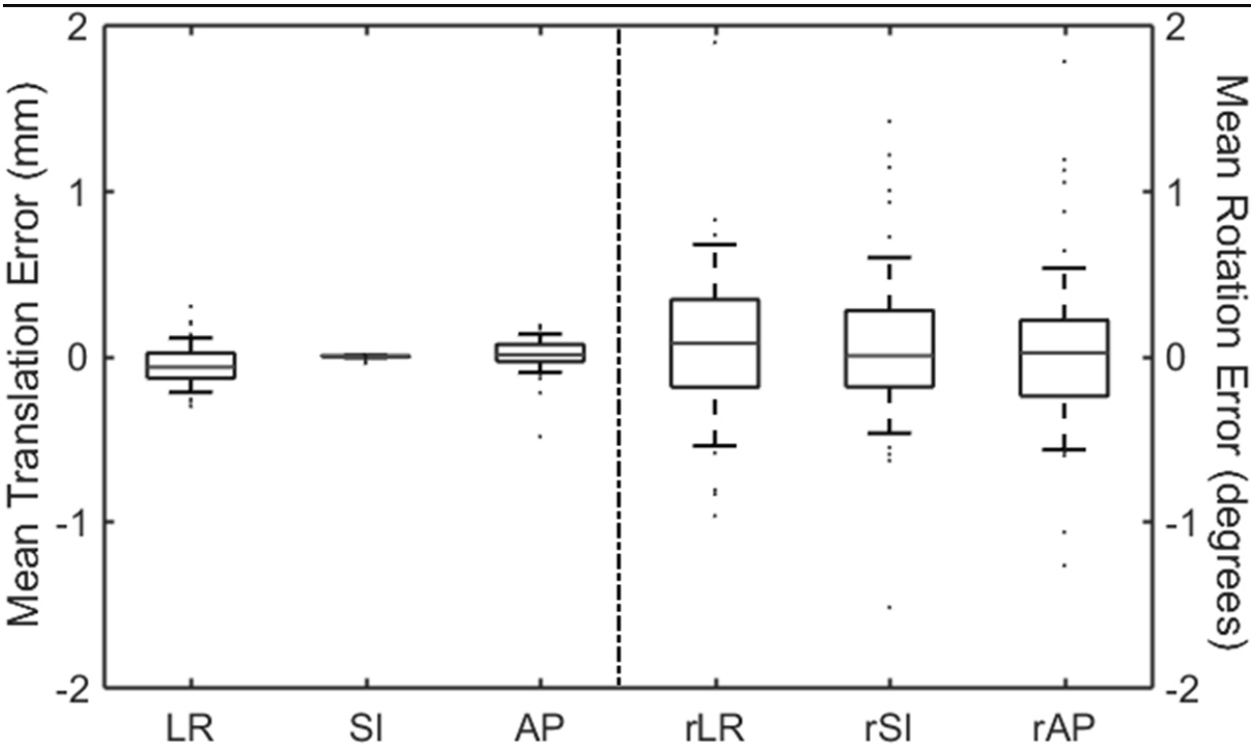

Figure 6. Boxplot showing the distributions of the mean error in each tested trace between 6D-IDC estimations of 6DoF motions with three markers and ground-truth across 81 liver tumour traces from 19 patients.

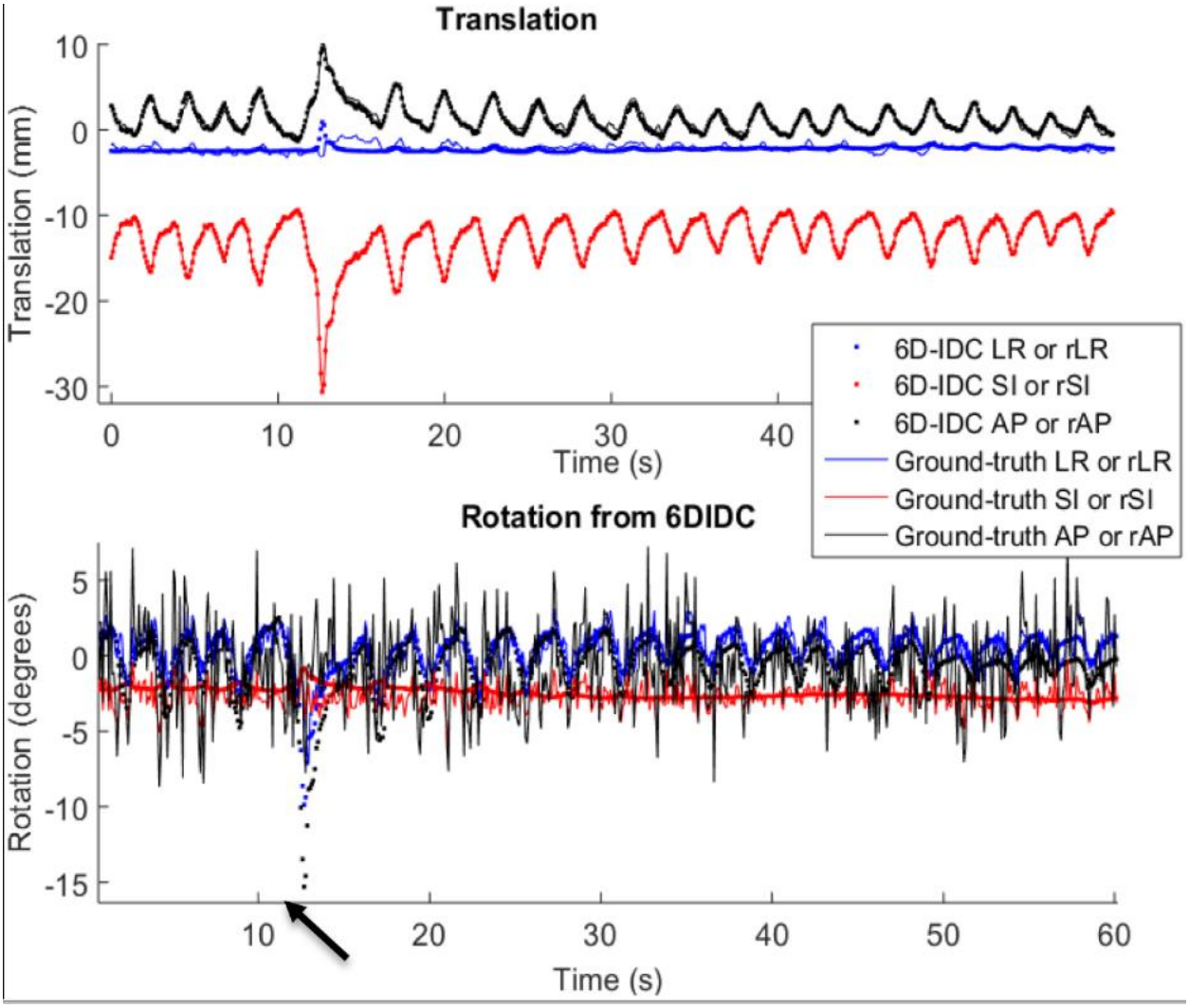

Figure 7. An example where 6D-IDC struggled in estimating motion due to a sudden change in correlation (arrow). The data from patient 14, fraction 1.

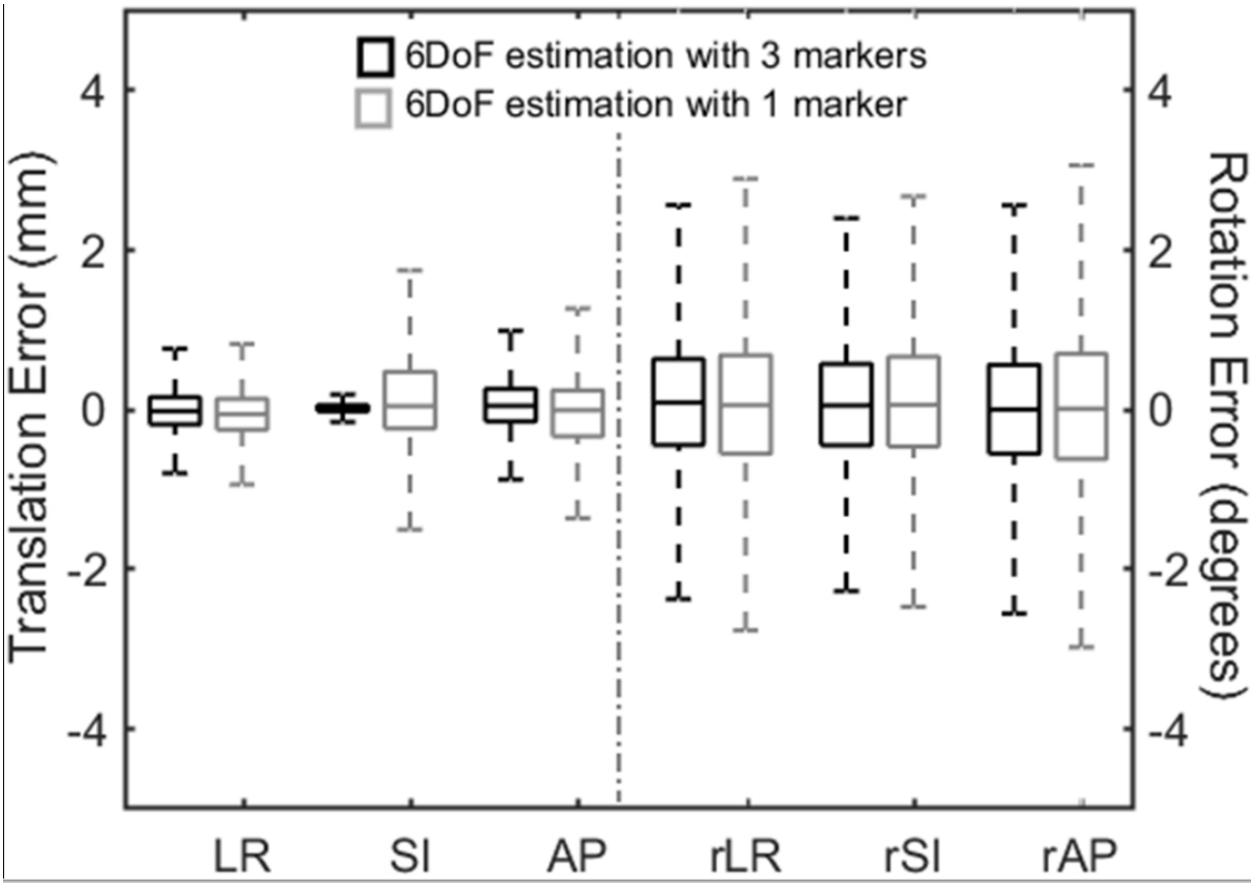

Figure 8. Boxplot showing the distributions of the mean of error in each segment in 6DoF between 6D-IDC estimation with projection of one marker versus projections of three markers after a learning arc across 81 liver tumour traces from 19 patients. The whiskers contains 99.9% of the data. Extreme outliers are not shown to highlight the difference between the two distributions.

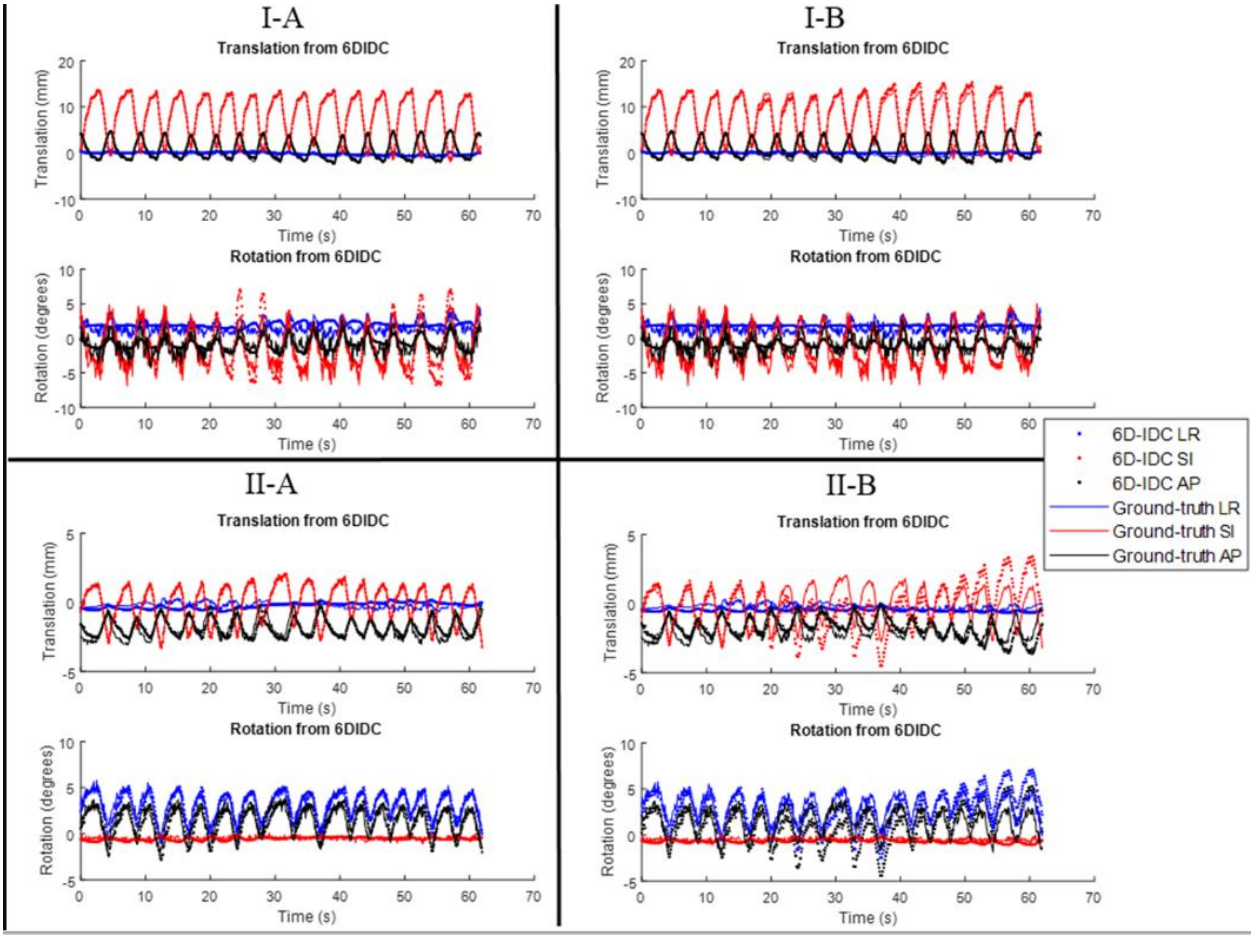

Figure 9. 6D-IDC estimation with projection of one marker versus with projections of three markers. (I) (Liver motion from patient 26, fraction 3): similar accuracy using three markers (I-A) and one marker (I-B). (II) (Liver motion from patient 1, fraction 3): 6D-IDC estimation using three markers (II-A) is more accurate than with only one marker (II-B).

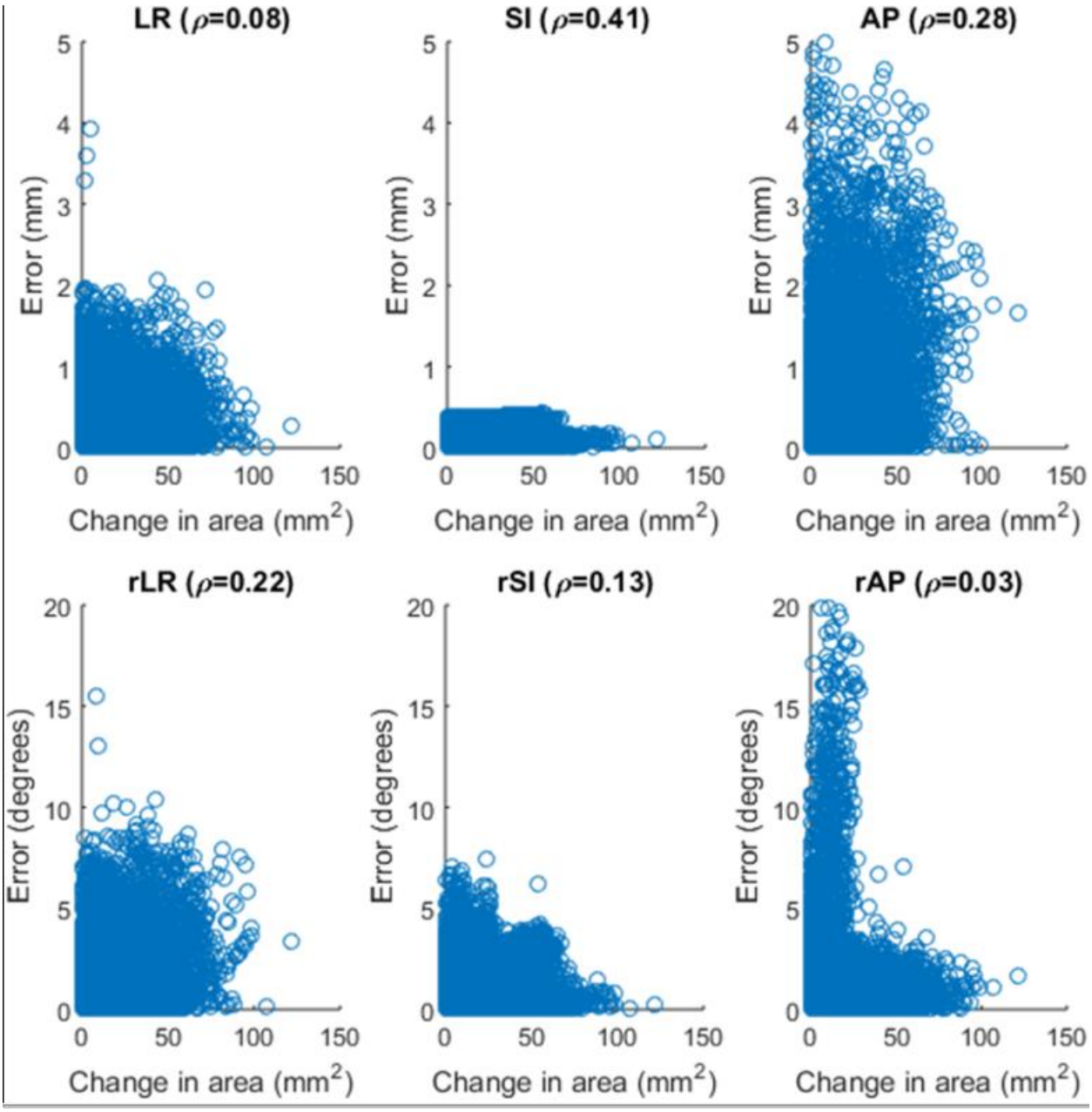

Figure 10. Scatter plots showing the relationship between the magnitude of errors and the magnitude of the change in the area made by the three fiducials. The ρ value indicates the Pearson correlation coefficient between each variables pair.

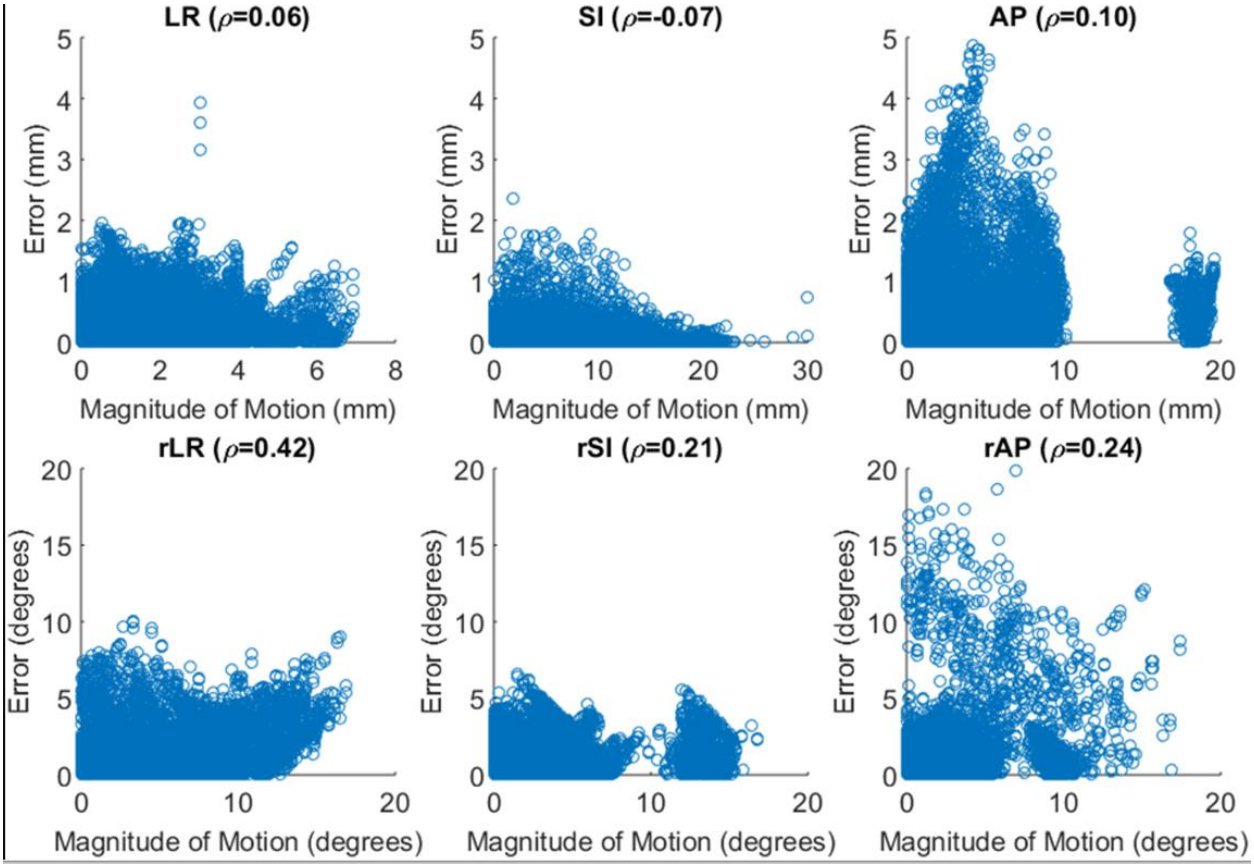

Figure 11. Scatter plots showing the relationship between the magnitude of errors and the magnitude of absolute motion of the target. The ρ value indicates the Pearson correlation coefficient between each variables pair.

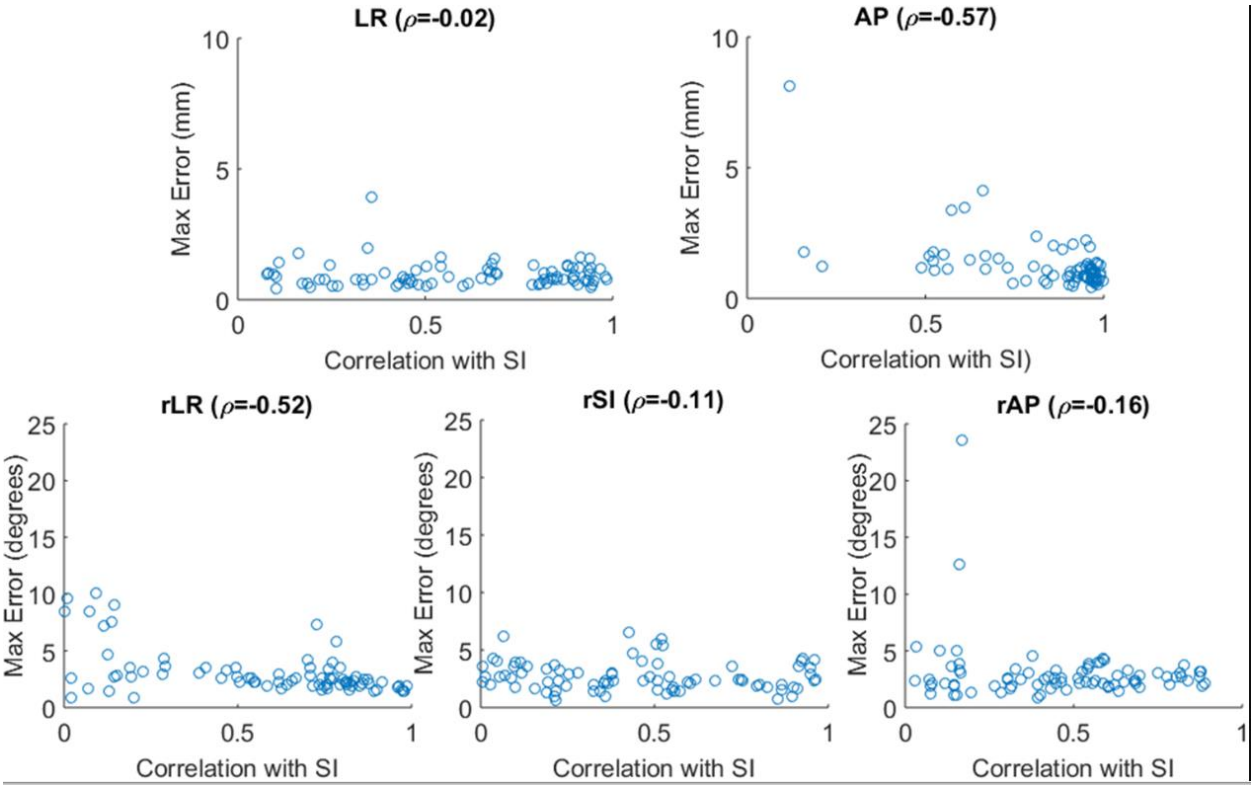

Figure 12. Scatter plots showing the relationship between the maximum error of 6D-IDC estimations in each degree of freedom and the absolute linear correlation value of the motion in that degree of freedom and the motion in the SI direction for each trace. The ρ value indicates the Pearson correlation coefficient between each variables pair.